The digital terrain model in the computational modelling of the flow over the Perdigão site: the appropriate grid size

José M.L.M Palma[1], Carlos A.M. Silva[1], Vitor M.C. Gomes[1], Alexandre Silva Lopes[1], Teresa Simões[2], Paula Costa[2], and Vasco T.P. Batista[1]

[1]Faculty of Engineering of the University of Porto (FEUP), Mechanical Engineering Department, Rua Dr. Roberto Frias, s/n, 4200-465 Porto, Portugal
[2]National Laboratory of Energy and Geology (LNEG), Estrada da Portela, Bairro do Zambujal, Apartado 7586, Alfragide, 2610-999 Amadora, Portugal

Correspondence: José M.L.M. Palma (jpalma@fe.up.pt)

Abstract. The digital terrain model (DTM), the representation of Earth's surface at regularly spaced intervals, is the first input in the computational modelling of atmospheric flows. The ability of computational meshes based on high (2 m, airborne laser scanning), medium (10 m, military maps) and low (30 m, shuttle mission, SRTM) resolution DTMs to replicate the Perdigão experiment site was appraised in two ways: by their ability to replicate the two main terrain attributes, elevation and slope, and by their effect on the wind flow computational results. The effect on the flow modelling was evaluated by comparing the wind speed, wind direction and turbulent kinetic energy by VENTOS®/2 at three locations, representative of the wind flow in the region. It was found that the SRTM was not an accurate representation of the Perdigão site. A 40 m mesh based on the highest resolution data, yielded at five reference points an elevation error of less than 1.4 m and an RMSE of less than 2.5 m, compared to 5.0 m, in the case of military maps and 7.6 m in the case of SRTM. Mesh refinement beyond 40 m yielded no or insignificant changes on the flow field variables, wind speed, wind direction and turbulent kinetic energy. At least 40 m horizontal resolution–*threshold resolution*–, and based on topography available from aerial survey, is recommended in computational modelling of the flow over Perdigão.

1 Introduction

A Digital Terrain or Elevation Model (DTM or DEM) is a representation of the Earth's surface elevation at regularly spaced
horizontal intervals. Although the terrain model is the first input in computational modelling of atmospheric flows, its impact
on flow results has not been a matter of concern, because the spatial resolution of publicly available DTMs is higher than the
size of the computational grid used to resolve the terrain. However, before a fluid flow database (Mann et al., 2017) can be
used as a reference in flow model appraisal and development, the impact of the terrain modelling must be assessed. For studies
of the atmospheric flow over Perdigão the publicly available DTMs were considered not accurate enough and an airborne laser
scanning campaign of the region was carried out in 2015, first to assist the design of the Perdigão campaigns in 2015 and 2017
(cf., Vasiljević et al., 2017; Fernando et al., 2019) and second, to provide the high resolution terrain data for computational
flow modelling, on par with the resolution provided by the large number of measuring equipment.

The Perdigão site is located in the municipality of Vila Velha de Ródão, in the centre of Portugal (608250E, 4396621N:
ED50 UTM 29N). It is comprised by two parallel ridges, about 500 m elevation, 4 km length, SE-NW orientation, and distanced
around 1.4 km from each other. The land is covered by a mixture of farming areas and patches of eucalyptus (*eucalyptus glob-
ulus*) and pine trees (*pinus pinaster*). The dominant winds are perpendicular to the ridges, assuring a largely two-dimensional
flow.

The accuracy of a DTM depends on the data collection techniques, data sampling density and data post-processing, such
as grid resolution and interpolation algorithms. In computational modelling of atmospheric flows, DTMs are often used
from photogrammetry or satellite interferometry, such as *SRTM, Shuttle Radar Topography Mission*, (Farr et al., 2007) or
ASTER, Advanced Spaceborne Thermal Emission and Reflection Radiometer (Yamaguchi et al., 1998), freely available at
https://earthexplorer.usgs.gov/. SRTM has the widest cover and is the most commonly used terrain data. Its latest version (V3.0
1", 2014) is 1 arc-second on most of the planet's surface, i.e. about 23.75 m resolution at Perdigão's latitude. With the advent
of high resolution techniques such as lidar aerial survey, terrain data has become available with resolutions above 10 m and the
question is whether such high resolution is needed in the computational modelling of atmospheric flows over complex terrain.

1.1 Literature review

Grid independent calculations is a concept very dear to computational fluid dynamics practitioners (e.g., Roache, 1998), as a
mean for reducing discretisation errors. However, its application in the context of atmospheric flows is not that simple, because
every level of grid refinement brings another level of surface detail; see for instance the coastline paradox (Mandelbrot, 1967,
1982). In this case, because the flow is driven by topography, the flow model results are directly correlated to the terrain
data and our problem is common to what can be encountered in geomorphology, with applications in hydrology (e.g., Zhang
and Montgomery, 1994; Deng et al., 2007), where the DTM grid size affects the drainage area. In spite of its importance, to
our knowledge, there is no systematic study on the appropriate grid size for resolving the terrain in microscale modelling of
atmospheric flow over complex terrain.

45   Work has been done in quantifying the impact of using different DTMs and resolution on terrain attributes, such as elevation, slope, plan and profile curvature, and topographic wetness index. For instance, Mahalingam and Olsen (2016) notes that DEMs are often obtained and resampled without considering the influence of its source and data collection method. Finer meshes do not necessarily mean higher accuracy in prediction (with examples for landslide mapping where terrain slope has a great influence) with the DEM source being an important consideration.

50   DeWitt et al. (2015) compares several DEMs (USGS, SRTM, a statewide photogrammetric DEM and ASTER) to a high-accuracy lidar DEM to assess their differences in rugged topography through elevation, basic descriptive statistics and histograms. Root mean square error values found ranged from 3 (using photogrammetric DEM) to circa 15 (using SRTM) or 17 m (using ASTER).

Deng et al. (2007) indicates that the mesh resolution can change not only terrain attributes in specific points but also the
55   topographic meaning of attributes at each point. It concludes that variation of terrain attributes were consistent with resolution change and that the response patterns were dependent on the landform classes of the area. Deng et al. (2007) introduce the concept of threshold resolution, i.e. the resolution beyond which the model quality deteriorated quickly, but below which no significant improvement in modelling results was observed.

Florinsky and Kuryakova (2000) develops an experimental three-step statistical method to determine an adequate resolu-
60   tion in DEM to represent topographic variables and landscape properties at a micro-scale (exemplified by soil moisture) by performing a set of correlation analysis between resolutions.

Diebold et al. (2013) show the effect of grid size in LES of flow over Bolund. Lange et al. (2017) addresses the question of how to represent the small topographic features of Bolund in wind tunnel modelling, comparing a round and a sharp edge of a cliff in a wind tunnel, to conclude that the flow with the sharp edge gives an annual energy production of a wind turbine near
65   the escarpment that is 20% to 51% of the round-edge case.

1.2   Objectives and outline

The objective of the present study is to determine the resolution required to accurately resolve the atmospheric flow over Perdigão and mountainous terrain in general. One needs to assess the terrain horizontal resolution before assessing the effect of other (also important) causes of differences between experimental and computational results. Many computational studies
70   based on Perdigão data are expected and it is important to asses the terrain resolution requirements first.

In what follows, we describe the techniques used for aerial and terrestrial surveying (section 2), plus the post-processing of those data and the determination of the main geometrical parameters of the Perdigão site (section 3). The results on terrain attributes and computational flow modelling are the subject of sections 4 and 5. The paper ends (section 6) with conclusions and recommendations on the most appropriate DTM and grid size required in the computational modelling of the flow over
75   Perdigão.

2 Topographical surveying: equipment and techniques

2.1 Airborne laser scanning (2015)

The lidar aerial survey was performed on 15 March 2015 by NIRAS (2015), with assistance from Blom TopEye. The survey covered an area equal to $22\,071\,075\,\mathrm{m}^2$ (Figure 1a) and was completed in one session, at an altitude of 500 m with a TopEye
80   system S/N 444 mounted on a helicopter. The number of points of the lidar point cloud was approximately 993198375, an average point density inside the project area equal to 45 points/m^2.

Lidar data was checked for point density control by TPDS (TopEye Point Density and Statistics), with the area being fully covered by lidar data with exceptions for watersheds. Concerning the primary data processing, the GPS data was processed using data from three Portuguese reference network stations (CBRA, MELR and PORT, cf. DGT (2017)), switched on 1 sec
85   registration after assistance by the Portuguese National Mapping Agency (*Direção-Geral do Território, Divisão de Geodesia*). Discrepancies between flight lines (based on Blom's software TASQ, TopEye Area Statistics and Qualities, calculated on subareas of 1 m and after matching of 204104275 observation) showed a maximum altitude deviation and RMSE equal to 0.490 m and 0.061 m. In 75% of the subareas the RMSE was lower than $60\,\mathrm{mm}$.

The photography (a total of 851 photos, stored as $300\,\mathrm{m} \times 300\,\mathrm{m}$ GeoTIFF files) was performed with a Phase One iXA180
90   camera, a medium format, 10328 pixel $\times$ 7760 pixel sensor resolution, yielding a ground resolution equal to $4.7\,\mathrm{cm}$. The delivery comprised orthophotos of $5\,\mathrm{cm}$ and $20\,\mathrm{cm}$ resolution (Figure 1b).

The prodution of the digital terrain model based on the lidar data is the subject of section 3.1.
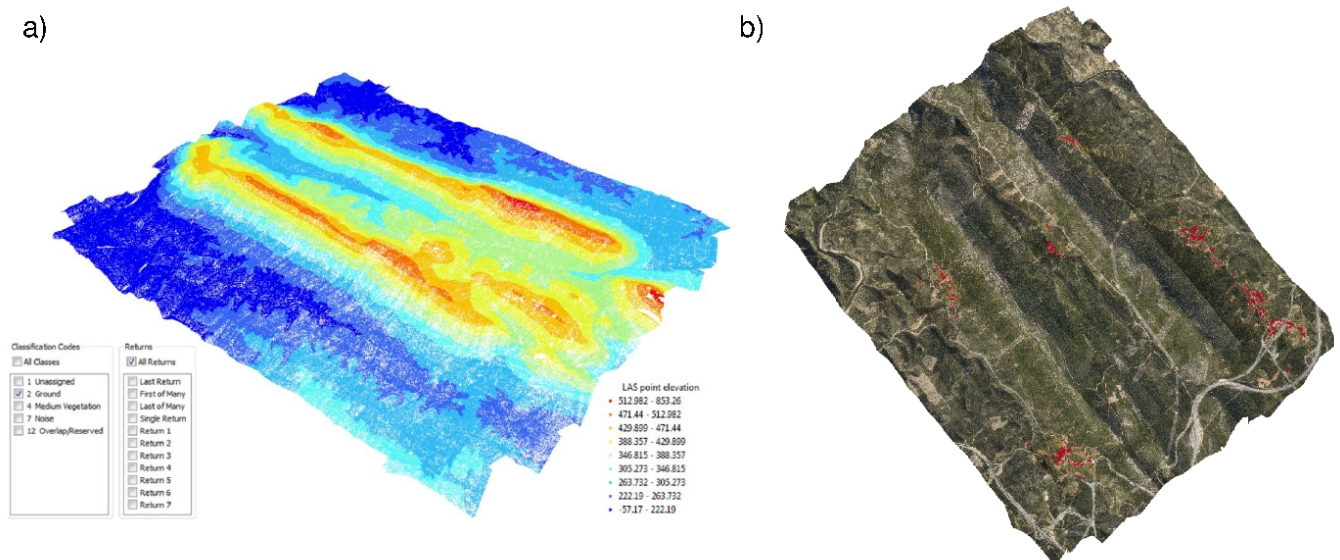
Figure 1. Lidar aerial survey and ortophoto.

2.2 Terrestrial surveying (2017 and 2018)

During the installation of scientific equipment (Nov 2016–May 2017), terrain elevation was measured in situ (Palma et al.,
95   2018) for an accurate and final determination of the elevation data of part of the instrumentation. The measuring equipment
was a Leica system, comprised of the following units: (1) Leica MultiStation MS50, (2) Leica Viva GS14 - GNSS Smart
Antenna, (3) Leica CRT16 Bluetooth Cap and (4) Leica GRZ121 360 Reflector PRO Surveying Prism.

In 2017, a piece of land required changes for installation of tower 20/tse04. The topographic survey of that region was
carried out (Alves, 2018) and incorporated in the lidar based terrain model as of March 2015. This survey was performed by
100 Spectra Physics (SP60 GNNS receiver and data collector T41 with Survey Pro software) equipment and software by Sierrasoft
(PROST Premium/Topko Standart, Version 14.3) for prodution of the local DTM at a 1:500 scale.

3   Terrain model

3.1   Airborne laser scanning (2015)

The lidar data was classified in laser pulse classes corresponding to four types of data (ground, vegetation, unassigned and
105 noise) and stored in LASer (LAS) File Format, and then post-processed by tools pertaining to the LAStools© software suite
(LAStools, 2019) in three stages, Figure 2.
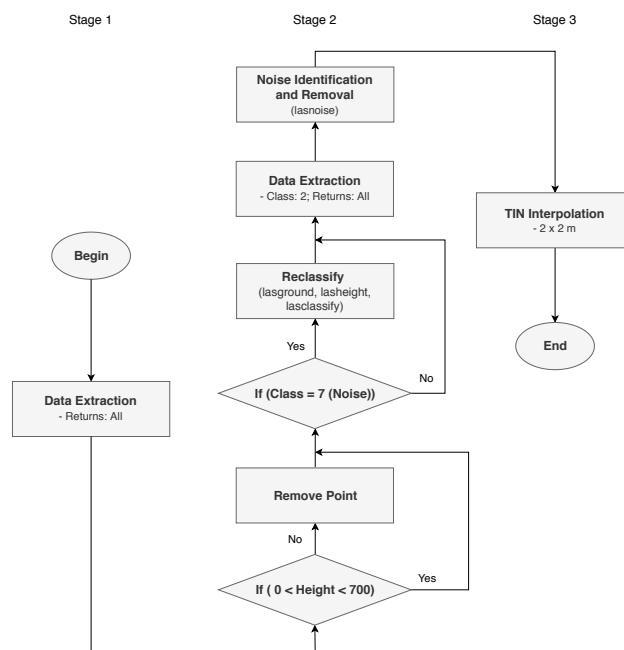
Figure 2. Workflow diagram for producing the terrain map using LAStools©.

Stage 1 was concerned with the extraction of the lidar raw data. The ground class data were mostly a mesh of regular spaced points, plus a few scattered points and small distinctive areas devoid of points, with abnormal values in their centre, attributed to lidar reading errors.

Stage 2 involved the reclassification of abnormal data. A first procedure was used to reclassify a particular area of noise-classified points into the ground or vegetation classes, which would otherwise be void of ground points. Points with excessive (>700m) or negative elevations a.s.l. were removed during this stage. Isolated points above or below the more spatially dense point cloud, classified as ground or vegetation, were identified and removed using the *lasnoise* tool.

In Stage 3, a Triangulated Irregular Network (TIN), based on the Delaunay triangulation, was obtained for the ground classified points. The DTM was obtained by interpolating the heights into a regular mesh with a resolution of 2×2 metre, the highest horizontal resolution of the terrain elevation within the Perdigão site.

3.1.1 Buildings

It is not clear whether a DTM should comprise buildings and other man-made artefacts that are usually part of digital surface models (DSM). In the context of the present study, buildings are long standing structures, as a terrain feature, and we first saw no reason for buildings not being part of the DTM. The houses, in Figure 1b, are family houses of about $15\,\mathrm{m} \times 15\,\mathrm{m}$ and $3\,\mathrm{m}$ height that will show on the finest mesh only and as a point elevation. Unless there are a few neighbouring buildings, the ability to resolve isolated houses is limited.

The first task to include the building data in the DTM, embraced the extraction of unassigned (section 3.1) data points to a point database, containing points representative of obstacles, buildings or other types of structures detected by the lidar and different from vegetation or ground points. The second task involved the digitalization of all buildings from the orthophotos. This process was needed to retain the building polygons as close as possible to their exact shape and exclude possible outliers captured by the automatic points extraction, and also to perform a more effective and precise interpolation of the data. The third and final stage was the interpolation of the buildings points included inside the digitized polygons for a continuous representation of the buildings. The interpolation scheme used in the ArcGIS platform (ESRI, 2016) was the natural neighbour method (Sibson, 1981), which preserves the shapes boundaries (Watson, 1994).

Calculations including the building data showed minor or no visible flow changes and were discarded.

3.2 Two-dimensionality and main geometrical parameters

One of the reasons why Perdigão was selected was its geometry; namely, the parallelism between the two ridges and their large length relatively to the width, bringing the orography close to two-dimensionality.

3.2.1 Area of interest (AOI), reference lines and locations

For scaling and dimensional analysis, the main geometrical parameters of the Perdigão site were determined and the area of interest (AOI) was defined (Figure 3 and Table 1): a rectangular shape of aproximately $(3\,\mathrm{km} \times 4\,\mathrm{km})$, with lower left corner

at 608589E; 4394131N and aligned with the centreline (ℓ_C, SE-NW direction, $135°$). This area, centred near station 131, included the SW and the NE ridge, the valley and the location of most of the instrumentation deployed in Perdigão. Note that

140   the coordinate system was converted from ETRS89 PT-TM06 (original source) to ED50 UTM29 and will be used throughout the document as Eastings and Northings. Stations number (#) and code as in Perdigão web site (perdigao.fe.up.pt/).
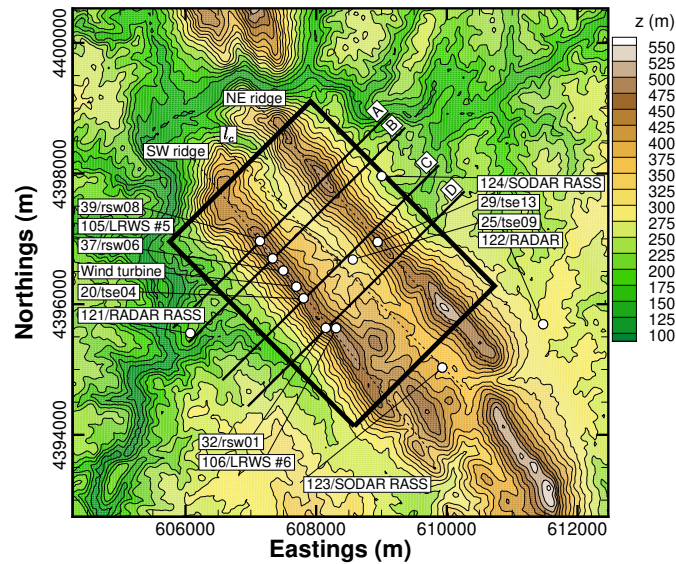
Figure 3. Area of interest and transects (ED50 UTM 29N).

3.2.2   Terrain profile and slope

The terrain profile (Figure 4) is not uniform along the valley, which becomes narrower and deeper along the SE-NW direction. For instance, the NW ridge height relative to a reference height (h_{ref}, the mean height of the surrounding terrain in a $20 \times 20\,\mathrm{km}$

145   area) equal to 250 m a.s.l. varies between 201.06 and 251.36 m, and the distance between ridges is 1358.00 and 1480.00 m on transects A and D (Table 2).

     Apart from ℓ_C, six additional lines were defined: ℓ_{SW} and ℓ_{NE} along the SW and the NE ridges, and A, B, C and D, perpendicular to the ridges (SW-NE direction, $225°$) and related to four main transects: A and D that delimit the northernmost (station 39) and southernmost (station 32) locations of the great majority of the instrumentation; and transects B and C that

150   delimit a narrower region, determined by locations of stations 105/LRWS#5 and 20/tse04.

     Other geometric variables (Figure 4) are the height of ridges (h_{SW} and h_{NE}) and valley (h_{val}) relative to the reference height (h_{ref}), the half-widths of the ridges ($l_{SWw}, l_{SWe}, l_{NEw}$ and l_{NEe}) at half-height ($h_{SW}/2$ and $h_{NE}/2$), and the distance between ridges, ℓ.

Table 1. Reference points as in Figure 3 (ED50 UTM 29N).

#	Type/Code	Eastings (m)	Northings (m)	Elevation (m)
	Wind turbine	607697.43	4396268.40	484.0
20	20/tse04	607808.15	4396089.94	473.0
25	25/tse09	608561.10	4396683.01	305.3
29	29/rsw01	608938.98	4396953.43	452.9
32	32/rsw01	608148.76	4395637.77	472.1
37	37/rsw06	607497.90	4396514.05	482.5
39	39/rsw08	607140.01	4396966.32	488.9
105	LRWS #5	607334.63	4396700.65	485.9
106	LRWS #6	608306.93	4395634.00	486.3
121	RADAR/RASS	606073.73	4395557.68	223.7
122	RADAR	611473.79	4395693.69	288.6
123	SODAR/RASS	609930.76	4395029.08	361.9
124	SODAR/RASS	609002.59	4397960.14	258.4
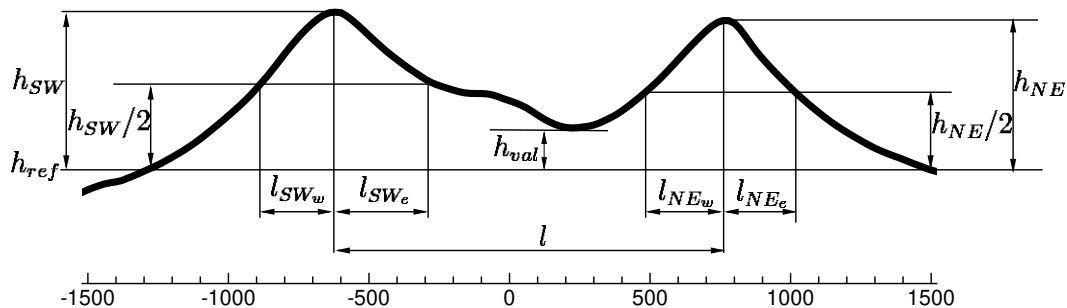
Figure 4. Terrain profile: geometrical parameters.

The ridges' orientation was determined by a linear regression of two z maxima, for each j (mesh oriented with SW-NE direction) on a $20\,\mathrm{m}$ grid, between transects A and D ($\approx 1650\,\mathrm{m}$) and between transects B and C ($\approx 530\,\mathrm{m}$). The deviations from parallelism are $4.3°$ if restricted to the region between A and D. Between transects B and C, where the core of the instrumentation was, the ridges were parallel within $2.8°$; i.e., $139.1°$ and $136.3°$ in the case of SW and NE ridges. The slope ($S = |\mathrm{atan}(h_{SW,NE}/2)|/\ell_{SW,NE}$), also on a $20\,\mathrm{m}$ grid varies between $21.08°$ and $45.09°$, always above the threshold for flow separation (Wood, 1995).

Table 2. Main geometric variables of transects A, B, C and D (slope (S) in degrees ($°$), and length and elevation (ℓ and h) in metre, $h_{ref} = 250$ m a.s.l.).

	A	B	C	D	Average
h_{SW}	237.22	237.32	228.26	221.96	231.19
h_{NE}	251.36	212.65	205.29	201.06	217.59
h_{val}	24.52	31.14	46.79	65.23	41.92
l_{SWw}	277.81	214.03	232.04	212.26	234.04
l_{SWe}	269.96	304.99	402.87	432.00	352.46
l_{NEw}	286.87	320.16	249.47	268.69	281.30
l_{NEe}	258.35	244.94	221.91	261.74	246.74
l	1358.00	1384.00	1412.00	1480.00	1408.50
S_{SWw}	33.64	37.47	36.78	39.99	36.97
S_{SWe}	-45.09	-29.60	-22.68	-21.08	-29.61
S_{NEw}	30.65	25.69	27.81	25.69	27.46
S_{NEe}	-35.74	-30.05	-30.65	-24.11	-30.14

4 Digital terrain model: results and discussion

The terrain elevation and slope are the two main terrain attributes for classification of terrain complexity and the ones to replicate accurately by terrain models. In this section, three DTMs of the Perdigão site are analysed within the AOI, by comparing terrain elevation and slope on meshes based on these terrain models with the terrain elevation and slope measured by the lidar aerial survey data within the AOI.

The three DTMs (Figure 5 and section 4.4) were the following: (1) ALS, the area sampled by lidar with a $2\,\mathrm{m}$ resolution (file #1 of Topography data on page 22); (2) Military, the Portuguese Army cartography around Perdigão, $10\,\mathrm{m}$ horizontal resolution (file #2 of Topography data on page 22) available from Portuguese Army Geospatial Information Centre (*CIGeoE Centro de Informação Geoespacial do Exército*), a total of eight sheets (numbers 290.4, 291.3, 302.2, 302.4, 303.1, 303.3, 313.2 and 314.1) at a scale equal to 1:25000; and (3) SRTM, the SRTM 30 m (file #3 of Topography data on page 22).

Because the ALS was the highest resolution map, and the most accurate representation of the terrain in Perdigão, it was the one against which the accuracy of alternative terrain data sources was evaluated.

Concerning the terrestrial surveys in 2017 and 2018 (section 2.2), a sample of those measurements confirmed the high quality of lidar airbone measurements. The survey carried in 2018, showed that the terrain change due to installation of tower 20, yielded alteration of the terrain that were not significant (lower than 1 m).

4.1 Mesh generation

For comparison of terrain attributes, elevation and slope, regularly spaced meshes of 80, 40, 20 and 10 m (size, $n_i \times nj$, respectively 39×51, 77×101, 153×201 and 305×401) were generated within the AOI. The resampling procedure was
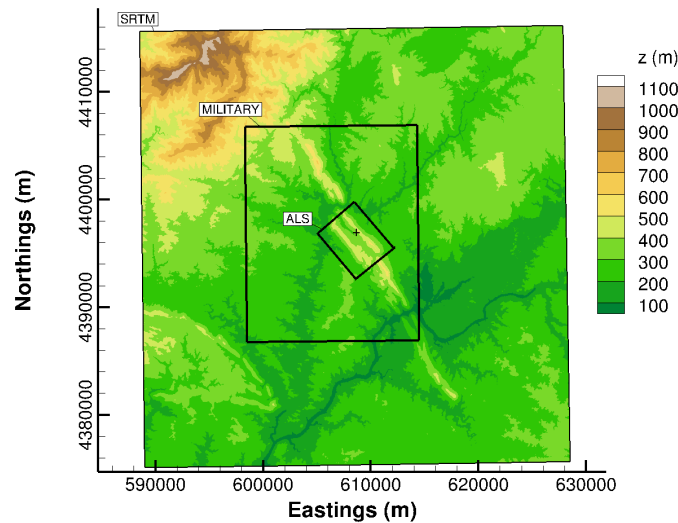
Figure 5. Total area comprised by SRTM, military and airborne data (+: domain centre).

similar to Deng et al. (2007); i.e., one out of two points was retained to assure that every point in the coarser resolutions existed on the finer ones. Coarser meshes are resampled versions of the 2 m resolution mesh, obtained by removing additional nodes.

4.2 Elevation at five reference points

Five points (Table 1) were selected for DTM comparison: towers 20/tse04, 25/tse09 and 29/tse13, the three 100 m meteorological towers, comprising a transect aligned with the dominant wind direction, and tower 37/rsw06 and the wind turbine location, along the SW ridge.

Figure 6 shows the absolute error ($z_{error} = z_{80,40,20,10} - z_2$), difference between the elevation at a given mesh and DTM source, with respect to the terrain elevation on the reference mesh (ALS$_2$). In the case of SRTM based meshes (Figure 6a), the error tends to a plateau at resolutions equal to 40 m. Similar behaviour is found in the case of the Mil database (Figure 6b), but at 20 m resolution; 20 and 10 m mesh increases the error at 20/tse04 and meshes at higher resolution to the uncertainty of this database must be avoided. Contrary to the SRTM and Mil, when using ALS (Figure 6c), with mesh refinement there is a noticeable error reduction at all 5 points.

4.3 Elevation and slope in the area of interest (AOI)

As the DTM quality increased from SRTM to Mil and ALS, the maximum terrain elevation (z_{Max}) also increased, from 530.2 to 540.5 and 540.8 m, and the minimum (z_{Min}) decreased from 165.0 to 158.8 and 150.7 m (Table 3). Maxima and minima
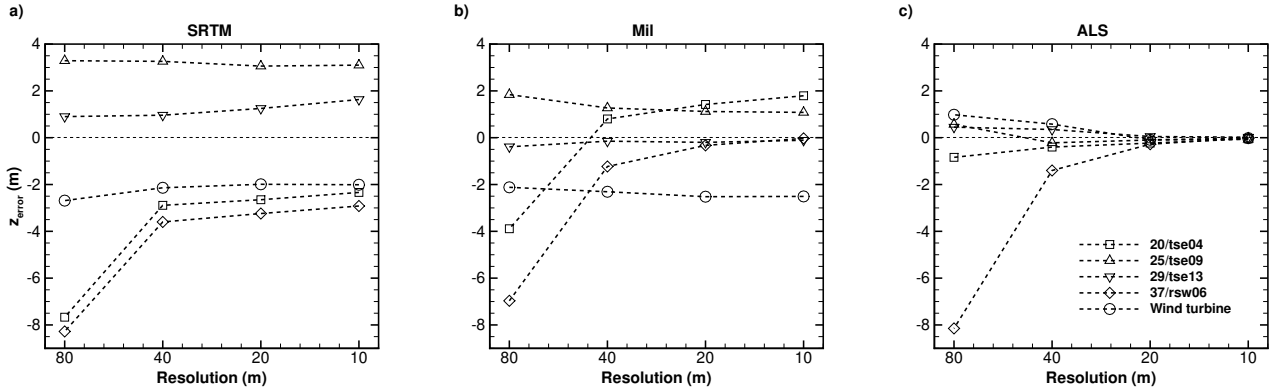
Figure 6. Impact of mesh resolution on reference points: a) SRTM; b) Mil; c) ALS.
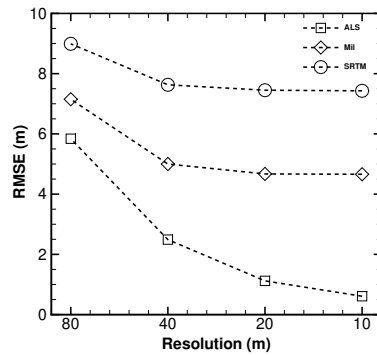
Figure 7. Impact of mesh resolution on RMSE.

terrain elevations are set by the DTM source; maxima and minima are similar for a given DTM regardless of the grid size, which was a consequence of the procedure for mesh refinement.

Table 3. Maxima and minima terrain elevation, based on SRTM, Mil and ALS data.

Mesh	z_{Max} (m)			z_{Min} (m)		
	SRTM	Mil	ALS	SRTM	Mil	ALS
80	530.2	538.4	537.3	165.0	159.4	146.0
40	530.2	538.4	537.9	165.0	159.4	149.2
20	531.1	540.0	539,4	165.0	158.8	150.3
10	531.4	540.5	540.8	165.0	158.8	150.7
2	-	-	541.1	-	-	155.2
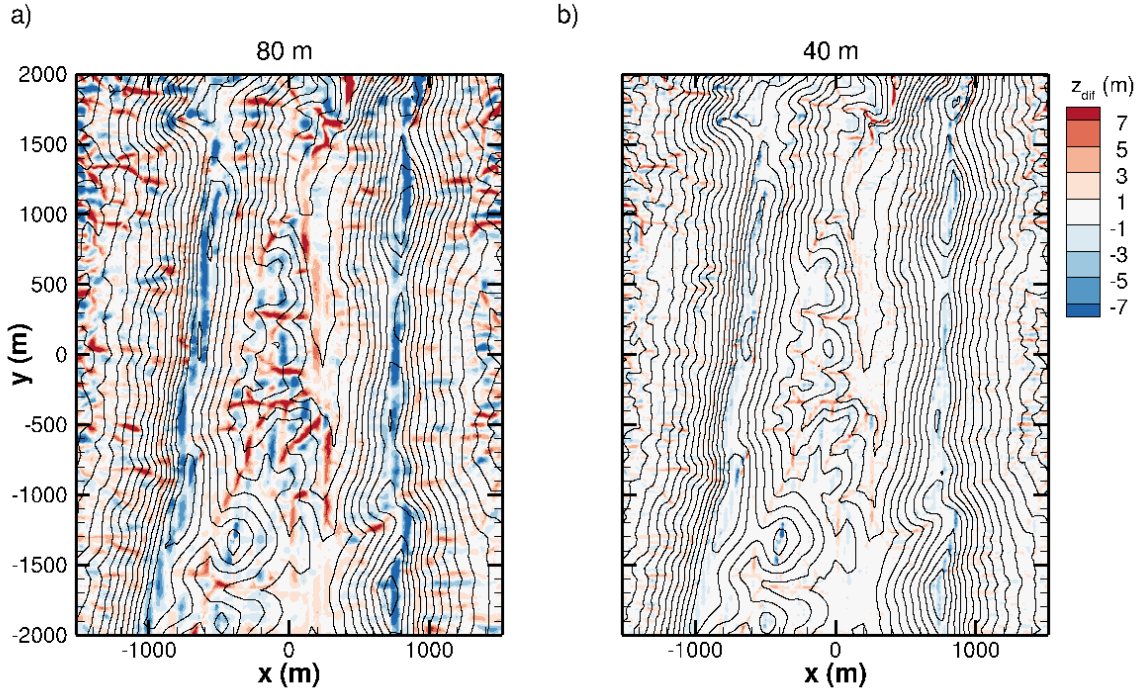
Figure 8. Elevation error of resampled meshes (ALS terrain data) over the AOI surface: a) 80 m mesh; b) 40 m mesh

.

Table 4. Maxima and minima slope in the x (SW-NE, 225°) direction, based on SRTM, Mil and ALS terrain data.

	S_{Max} (°)			S_{Min} (°)		
Mesh	SRTM	Mil	ALS	SRTM	Mil	ALS
80	39.00	38.27	37.31	-36.11	-37.99	-37.33
40	41.61	43.10	44.24	-38.64	-47.61	-51.74
20	44.65	49.36	55.85	-47.18	-55.19	-59.31
10	47.86	51.74	64.76	-49.02	-61.31	-67.81
2	-	-	75.91	-	-	-81.13

195   The error distribution (Figures 8 and 10a) shows an overprediction of the terrain elevation along the valley and an underprediction along the ridges, with both much reduced between the 80 and the 40 m resolution meshes, with the latter showing a mostly uniform error distribution of around 1 m (Figure 8b).

The RMSE error (Figure 7) over the whole AOI is consistent with the elevation error and the inherent uncertainty of every DTM source; with mesh refinement every DTM tends to its resolution level. The minimum RMSE of SRTM, Mil and ALS are
200   7.43, 4.66 and 0.61 m at resolutions of 10 m.
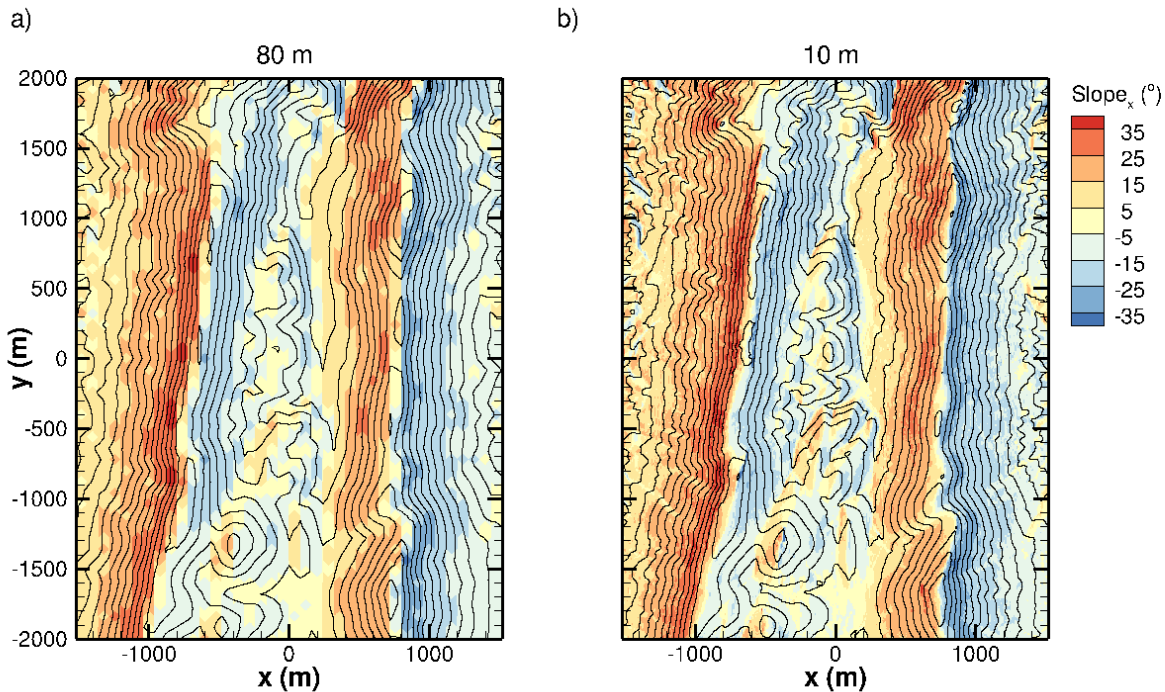
Figure 9. Slope in x (SW-NE, 225°) direction with different resolutions mapped on AOI's surface (ALS terrain data): a) 80 m mesh; b) 10 m mesh

.

The maximum slope (55.85° and 64.76°) was about 50% higher on 20 and 10 m meshes compared with the coarser resolution (37.31° and 44.24° meshes, 80 and 40 m), Table 4. The negative slope increased from −37.33° to −67.81°, as the resolution increased from 80 to 10 m. The histogram of the slope in the x (SW-NE, 225°) direction (Silva, 2018) shifted to the right, as the content at low slopes, decreases and more and more higher slope locations were resolved. Because the ridges are quasi two-dimensional, the y (SE-NW, 135°) direction slope was residual (Silva, 2018) compared to the x direction slope (Figure 9) and is not shown here.

The larger errors occurred at locations of higher slope (Figure 10) and these are the locations where the grid refinement was also the most effective in reducing the elevation error. For instance, errors equal to $11.5\,\text{m}$ and $-15.8\,\text{m}$ (at $x = -720\,\text{m}$ and $x = 766\,\text{m}$) on a 80 m mesh were reduced to $7.5\,\text{m}$ and $-2.5\,\text{m}$ on a 40 m mesh.

4.4 Spectra analysis

Spectra of terrain elevation show the ALS resolution one order of magnitude higher compared to SRTM data (Figure 11). The figure also displays two scaling ranges, typical of global topographies (e.g., Nikora and Goring, 2004), with exponents equal to -7/4 and - 11/3.
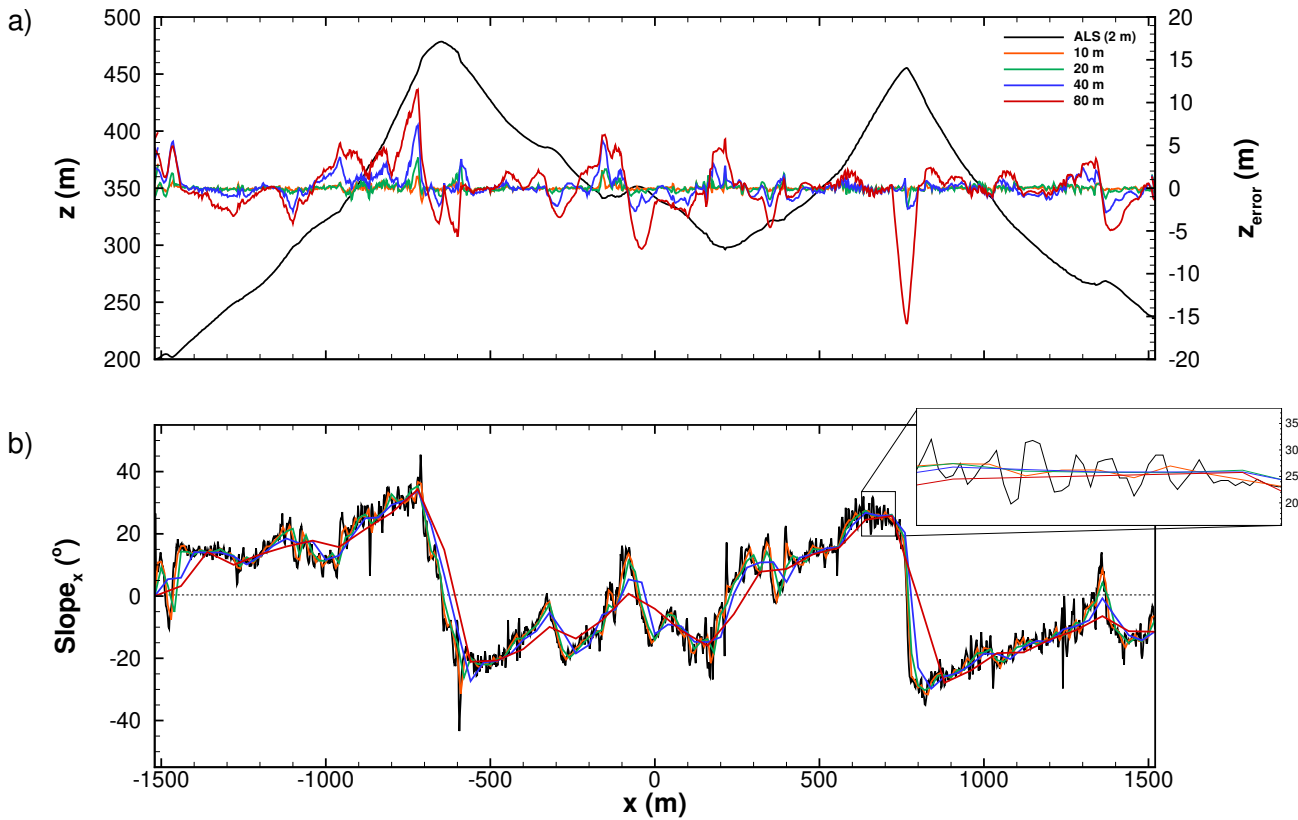
Figure 10. Elevation and slope in the x direction profiles on a plane that contains tower 20/tse04 (ALS terrain data).

As expected, there is an increase in resolved spectral range with mesh refinement and an overlap between meshes with ALS

215 data. In the case of SRTM and Mil based meshes, linear refinements (20 and 10 m meshes) cannot replicate the decay for higher

frequencies and overcome the inherent resolution of the original data. Mesh quality was as good as the terrain data source. Only

meshes based on the ALS have the ability to reproduce accurately the high-frequency range ($10^{-1}\,\mathrm{rad\,m^{-1}} < k < 1\,\mathrm{rad\,m^{-1}}$).

SRTM is restricted to around 30 m resolution and meshes 20×20 and 10×10, with identical z_{Max} and z_{Min} (531 and 165 m),

are unable to replicate the ALS measured values, z_{Max} and z_{Min}, Table 3. Grid refinement cannot go beyond the inherent

220 resolution of the DTM.

4.5 RIX (ruggedness index)

The RIX (ruggedness index) is one of the major parameters in WAsP (Mortensen et al., 2004). It has the goal of quantifying the

terrain complexity. The operational envelope of WAsP corresponds to a RIX value of 0%. The ALS data shows a maximum of
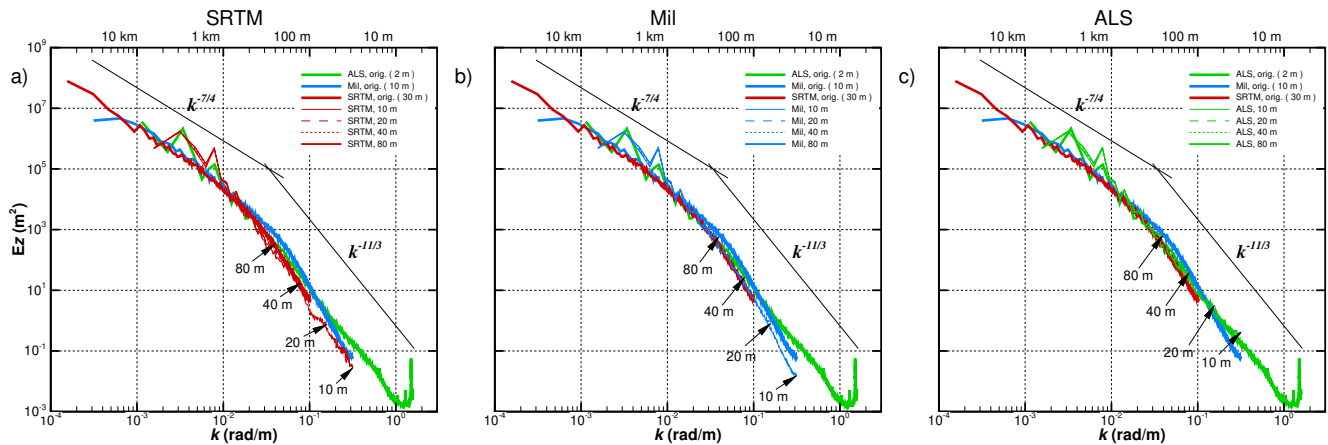
Figure 11. Spectra analysis for DTM and meshes.

23.7% and an overall higher value of RIX (average 15.22%), while SRTM reaches 19.7% (average 11.06%). Lower resolution
225   terrain data underestimate the terrain complexity.

5   Flow modelling

In this section, the results of computational runs on different meshes are discussed. A set of experimental data (30 minutes
averaged) on 4 May 2017, 22:09–22:39 UTM is also included, for guidance only; because computational results do not con-
sider, for instance, surface cover heterogeneity or stratification, discrepancies are expected when compared with experimental
230   data. This was the day and the time when the assumption of conditions of both stationarity and neutral flow in Perdigão could
be made, according respectively with Carvalho (2019) and Palma et al. (2019), and therefore approach the steady-state regime
and neutral atmospheric conditions of the computational runs.

5.1   Computational flow model

The computational code VENTOS®/2 (cf., Castro et al., 2003; Palma et al., 2008), developed for atmospheric flows over
235   complex terrain, was used in steady state formulation. It solves the RaNS set of equations for a turbulent flow ($\kappa - \varepsilon$ model),
with a terrain-following structured mesh, allowing also the simulation of forested terrain and wind turbines.

5.1.1   Integration domain and boundary conditions

The model topography (domain size, $19\,\text{km} \times 18.8\,\text{km}$, around the central location 608250E, 4396621N) was obtained by
bi-linear interpolation of terrain data. The positioning of the domain boundaries and its impact on flow variables were part of
240   the work of Silva (2018).

At the inlet a log-law profile was set. To ensure an equilibrium shear stress, the k profile decreases with the square of height above ground level. At the top of the domain a zero shear stress condition was used. The inlet profile's development is caped at the boundary layer's limit, all quantities being constant above that height. At the lateral boundaries a symmetry condition was applied.

245 The ground was modelled as a rough surface, a wall function, a log-law defining the velocity at the node closest to the ground, and the turbulence model quantities, k and ε. The values used in the computational model for z_0 (roughness length) and u_* (friction velocity) were 0.1 (indicated by Wagner et al. (2019) as the roughness length near the double ridge area after conversion from the CORINE Land Cover classes) and 0.25. These values were uniform for the whole domain. The surface cover (forest patches and height) and its representation in the computational model (roughness length, leaf area index, use of a

250 canopy model) is still a work in progress, as the presence of eucalyptus and pine tree patches in the area are expected to have a decisive impact on the flow.

5.2 Computational meshes

A total of 18 computational meshes (Table 5) was used. The central part of the domain ($4\,\mathrm{km} \times 6\,\mathrm{km}$, based on ALS and Mil terrain data), was resolved with uniform horizontal resolution ($20 \times 20, 40 \times 40$ and 80×80 m), expanding towards the

255 domain boundaries with factors f_x and f_y close to 1, to minimise the discretisation errors. The domain's height (3000 m) was discretised by 100 nodes (n_k), with the first node 2 m above ground level and a grid expansion $f_z = 1.0435$, yielding a maximum cell size (Δ_z) equal to 124 m.

A preliminary analysis showed that the flow variables had low sensitivity to the number of nodes in the vertical (n_k), opposed to the height of the first node above ground level, which showed a significant impact and is worthy of further studies.

260 Three types of meshes were used: SRTM, with the whole domain based on the SRTM data; Mil, a combination of SRTM and Military maps; and ALS, based on all three DTM sources (Figure 5). A minimum of 8818 iterations and 3.87 hours of computing time were required, and a maximum of 20033 iterations and $50\times$ more computing time in the case of mesh Mil.NE.20. Number of iteration is a better indicator of the actual computing time, since the value given here was influenced by the computer load at the time of the calculations.

265 5.3 Flow pattern

The flow modelling analysis was based on the flow patterns at two transects in the case of SW and NE winds (Figures 12 and 13) and wind speed, wind direction and turbulent kinetic energy results for SW (Figures 14–16).

As expected, the flow pattern (Figures 12 and 13) is characterised by separated flow regions in the leeside of either ridges. The figures are coloured by the spanwise velocity component (v), showing two different streams: up-valley on the leeside of

270 SW ridge and down-valley on the upwind side of NE ridge (Figure 12) and down-valley in the case of NE winds (Figure 13).

The ridge height increases with the grid resolution (see insets) and the detachment point also moves to higher elevations, yielding longer and deeper separated flow regions, see for instance Figure 13. In the case of SW winds (Figure 12) the 20 and

Table 5. Computational meshes ($\Delta z_{Min} = 2\,\mathrm{m}$).

	Name	$\Delta_{x/y}$		$n_i \times n_j$	t_{CPU}	N_{iter}
		min	Max			
		(m)	(m)		(h)	
1	SRTM.SW.80	80	478.6	120×155	6.27	8818
2	SRTM.SW.40	40	400.0	200×270	52.96	11557
3	SRTM.SW.20*	20	414.0	320×470	-	-
4	Mil.SW.80	80	478.6	120×155	18.13	8906
5	Mil.SW.40	40	400.0	200×270	89.64	11040
6	Mil.SW.20	20	414.0	320×470	237.35	14095
7	ALS.SW.80	80	478.6	120×155	3.87	8898
8	ALS.SW.40	40	400.0	200×270	15.09	10996
9	ALS.SW.20	20	414.0	320×470	111.28	16606
10	SRTM.NE.80	80	478.6	120×155	19.92	9554
11	SRTM.NE.40	40	400.0	200×270	110.04	14227
12	SRTM.NE.20	20	414.0	320×470	242.57	15188
13	Mil.NE.80	80	478.6	120×155	28.43	9313
14	Mil.NE.40	40	400.0	200×270	101.90	13351
15	Mil.NE.20	20	414.0	320×470	191.38	20033
16	ALS.NE.80	80	478.6	120×155	3.74	9322
17	ALS.NE.40	40	400.0	200×270	93.49	11937
18	ALS.NE.20	20	414.0	320×470	80.21	18634

Expansion factors			
$\min(\Delta_{x/y})$	f_x	f_y	f_z
80	1.0524	1.0331	1.0435
40	1.0471	1.0299	1.0435
20	1.0518	1.0271	1.0435

* Did not meet residual criteria

40 m resolution meshes yield similar results and appear to be accurate enough for computational modelling of atmospheric flow over Perdigão.

5.4 Southwesterly winds

The wind speed, wind direction and turbulent kinetic energy profiles at towers 20/tse04, 25/tse09 and 29/tse13 (Figures 14, 15 and 16) show that in general, there was a poor agreement with the measurements: wind speed underprediction at all towers,
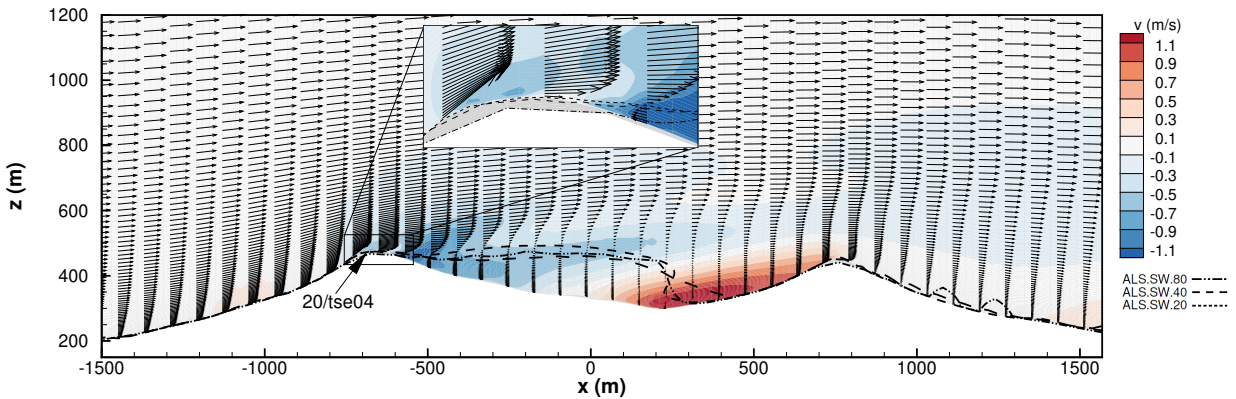
Figure 12. Impact of mesh resolution on separation zone in transect that crosses Tower 20/tse04.
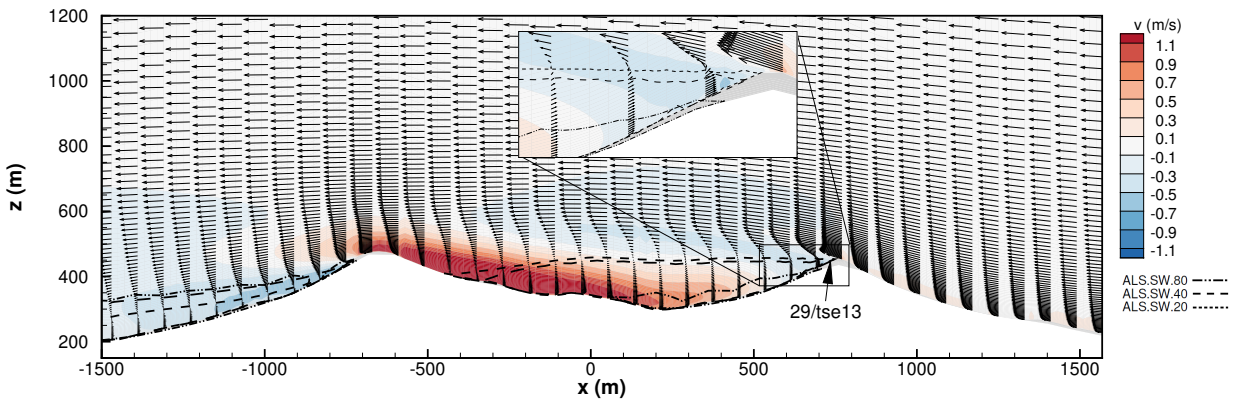
Figure 13. Impact of mesh resolution on separation zone in transect that crosses Tower 29/tse13.

whereas turbulent kinetic energy was overpredicted at the top of the SW ridge (20/tse04, Figure 14c) and underpredicted in the valley and at the NE ridge (25/tse09 and 29/tse13, Figures 15c and 16c).

280   Lower wind speed at tower 20/tse04 (Figure 14a) is an indication that the inlet conditions and wall parameters (z_0 and u_*) were too high, yielding a high loss of momentum along the 10000 m upstream of this tower. Computational results showed a good approximation to wind direction profiles for the three towers, little or no flow deviation was found between the inlet, the top of the southern ridge (tower 20/tse04) and the top of the northern ridge (tower 29/tse04).

Tower 25/tse09 (Figure 15a) is inside the separated flow region, which explains the low wind speed. This separated flow
285 region is characterised by a rotation of the wind with the distance above the ground. The flow in the valley is aligned with the

valley and therefore perpendicular to the ridges and the incoming wind. For some reason, in the valley the best agreement with the experimental data occurred in the case of the coarser meshes.

As a whole, results depend more on the resolution than on the DTM and at least a resolution of 40 m is required. Differences between the computational results on 20 and 40 m resolution meshes are minor and within the uncertainty of computational modelling.
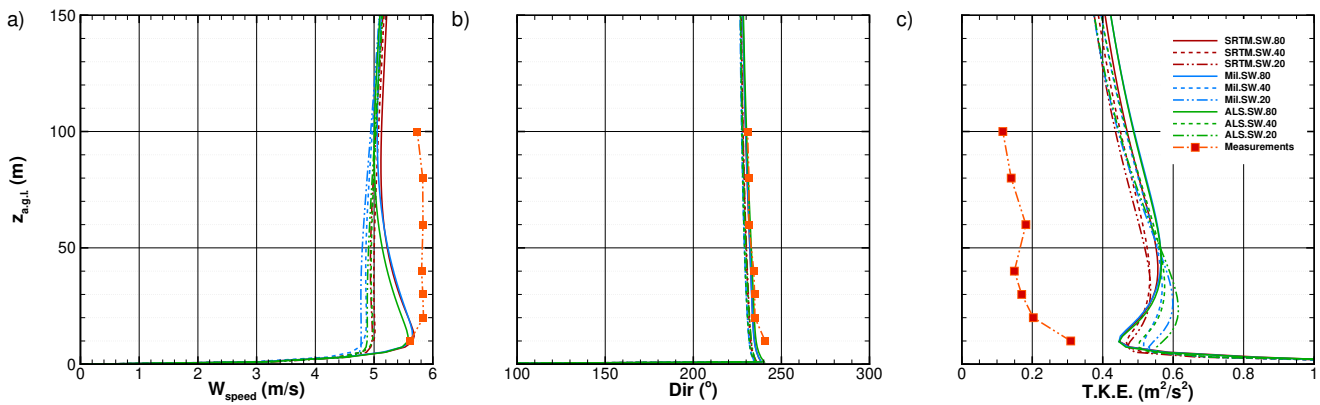
Figure 14. Wind speed, direction and turbulent kinetic energy profile simulation results in tower 20/tse04 for SW winds.
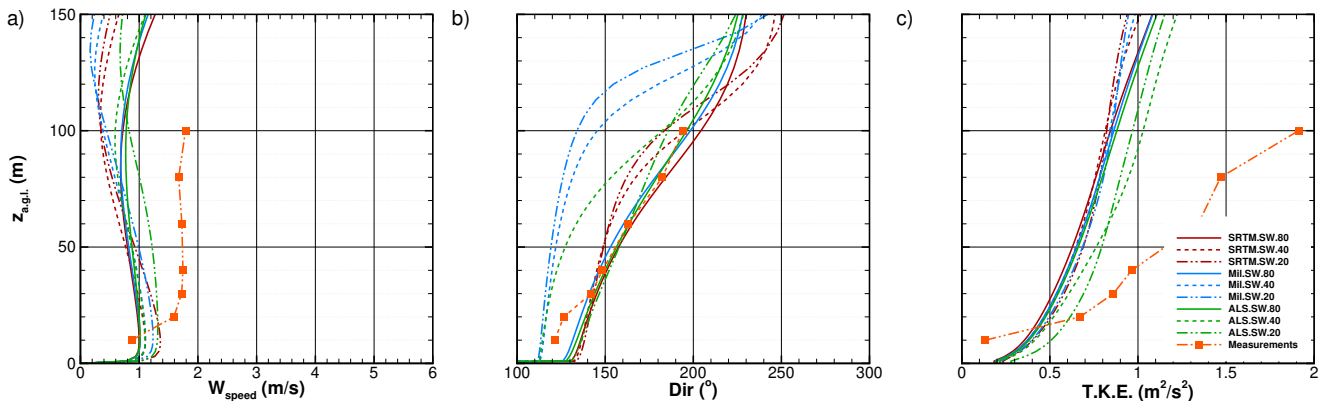
Figure 15. Wind speed, direction and turbulent kinetic energy profile simulation results in tower 25/tse09 for SW winds.

290

The profiles (not shown) in the case of NE winds ($45°$) are similar to SW winds, apart from the situation being reversed, since in this case the first and second ridge are the NE and SW ridges.

Differences between the profiles and the reference profile ALS_{20} were measured in terms of RMSE (Tables 6, 7 and 8) where a pattern similar to the slope (Table 4) can be observed. The effect of calculations on 20 m mesh are minor. Here we can see

295 again the limitations of the SRTM data, with RMSE higher than the cases based on either the military or the ALS data, 52% of the instances. And a threshold resolution around 20 and 40 m, depending on the variable.
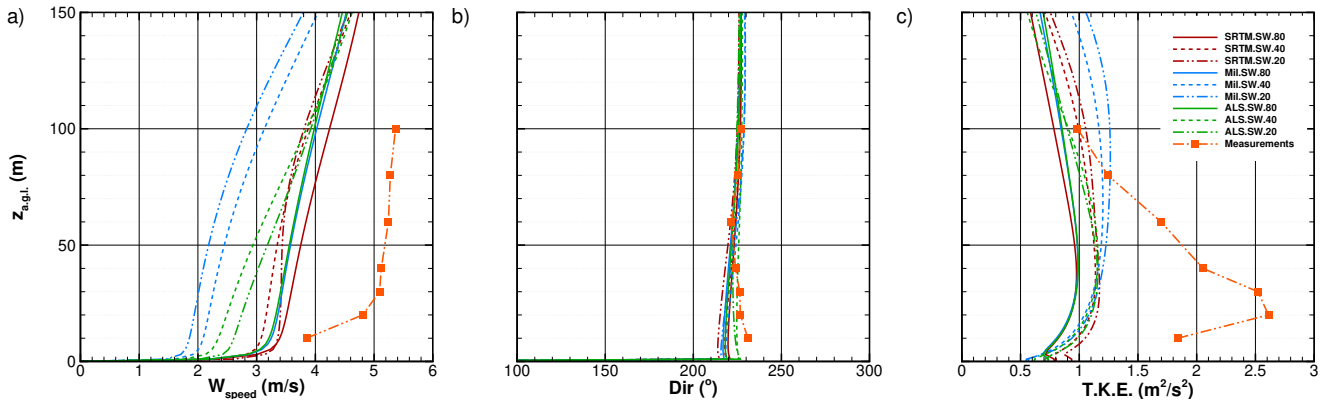
Figure 16. Wind speed, direction and turbulent kinetic energy profile at tower 29/tse13 for SW winds.

Table 6. RMSE of wind speed, wind direction and turbulent kinetic energy for tower 20/tse04.

	W_{speed} (m/s)			Dir (°)			T.K.E (m^2/s^2)		
	SRTM	Mil	ALS	SRTM	Mil	ALS	SRTM	Mil	ALS
				Southwesterly winds					
80	0.83	0.81	0.68	4.60	4.65	6.28	0.13	0.14	0.13
40	0.20	0.17	0.12	0.79	1.70	1.60	0.12	0.08	0.07
20	0.09	0.21	–	0.71	1.80	–	0.11	0.03	–
				Northeasterly winds					
80	1.28	2.53	2.43	16.80	16.49	14.90	0.78	1.01	1.04
40	0.99	0.50	0.22	9.84	9.83	4.09	0.46	0.33	0.39
20	0.18	0.30	–	5.04	2.74	–	0.06	0.08	–

6 Conclusions

Meshes for computational modelling of flow over the Perdigão site were created, based on three digital terrain models: high-resolution (2 m resolution) airborne lidar survey (ALS), Military (10 m) and SRTM (30 m) data. The mesh appraisal was
300 carried out in two ways: by their ability to replicate the two main terrain attributes, elevation and slope, and by their effect on the wind flow computational results (wind speed, wind direction and turbulence kinetic energy). About the digital terrain models, the main conclusions were the following:

1. The SRTM data is not an accurate representation of the Perdigão site.

2. Only meshes based on the ALS have the ability to reproduce the smaller scales between 10 and 100 m.

305 3. The ALS data yielded the lowest elevation errors; average RMSE around 5.8 m on 80 m, decreasing to 0.6 m on 10 m mesh.

Table 7. RMSE of wind speed, wind direction and turbulent kinetic energy for tower 25/tse09.

	W_{speed} (m/s)			Dir (°)			T.K.E (m²/s²)		
	SRTM	Mil	ALS	SRTM	Mil	ALS	SRTM	Mil	ALS
	Southwesterly winds								
80	0.87	0.77	0.69	26.67	20.10	14.81	0.33	0.29	0.26
40	0.92	0.90	0.70	38.14	75.35	48.96	0.36	0.34	0.16
20	0.81	0.84	-	37.03	92.73	-	0.36	0.32	-
	Northeasterly winds								
80	2.82	3.67	3.54	157.07	158.04	153.56	0.25	0.49	0.49
40	0.39	0.88	0.53	88.82	79.37	69.95	0.51	0.33	0.23
20	0.19	0.17	–	40.61	43.20	–	0.22	0.15	–

Table 8. RMSE of wind speed, wind direction and turbulent kinetic energy for tower 29/tse13.

	W_{speed} (m/s)			Dir (°)			T.K.E (m²/s²)		
	SRTM	Mil	ALS	SRTM	Mil	ALS	SRTM	Mil	ALS
	Southwesterly winds								
80	1.19	0.82	0.77	4.87	7.16	5.92	0.33	0.28	0.27
40	0.51	1.68	0.44	6.30	8.45	6.05	0.16	0.52	0.10
20	0.83	2.33	-	10.40	10.03	-	0.28	0.70	-
	Northeasterly winds								
80	0.44	0.49	0.44	16.15	17.73	16.79	0.13	0.15	0.13
40	0.26	0.16	0.24	6.94	10.26	5.35	0.06	0.07	0.06
20	0.18	0.09	–	2.98	4.66	–	0.04	0.03	–

4. The RMSE for SRTM 30 m does not go below 7.4 m. A 40 m horizontal resolution based on the ALS data is enough to achieve an error below 1.4 m in five key locations and below 0.28 m using a 20 m mesh.

5. The maximum terrain slope was about $1.8\times$ higher ($-67.81°$) on a 20 m mesh resolution compared with an 80 m mesh resolution ($-37.33°$). An 80 m mesh does not accurately represent elevation and slope, mainly near the extreme elevation values (highs and lows).

The effect of the terrain model on the wind speed, wind direction and turbulent kinetic energy were the following:

1. In the case of SW winds, the mesh resolution effects on the first ridge were restricted to the first 100 m a.g.l., where mesh refinement decreased the wind speed and degraded the quantitative agreement with the experimental data, though replicating the profile shape.

2. Separated flow field in the valley is perpendicular to the main flow direction. This region increases in height and length with the mesh refinement.

3. The flow (mainly the wind direction) in the valley was the most affected by terrain resolution; low velocities (about $1\,\mathrm{m\,s^{-1}}$) are associated with large variations of wind direction within the first 150 m a.g.l..

320 Concerning the digital terrain models and meshes, the conclusions were the following.

1. It was found that 40 and 20 m meshes are resolutions –threshold resolution– beyond which no or insignificant changes occur both in terrain attributes, elevation and slope, and in the flow field variables, wind speed, wind direction and turbulent kinetic energy.

2. Furthermore, only 40 and 20 m meshes based on military and ALS are appropriate to describe the Perdigão site and
325 SRTM should be restricted to far away regions.

3. Meshes of at least 40 m horizontal resolution are recommended in computational modelling of the flow over Perdigão, and based on topography available from aerial survey.

Data availability. Three datafile types are available

Lidar scanning files :

330
    1. 5. Delivery information

    6.1 Coordinate system in plane and height: PT-TM06/ETRS89 / Altimetric Datum from Cascais

    6.2 File formats

    Laserdata: LAS 1.2

    2. Ortho mosaic:

335
    3. This delivery includes a lidar point cloud, and 5 cm and 20 cm orthophotos.

Topography data :

    1. DTM of Perdigao site, terrain elevation on a regularly spaced $2\,\mathrm{m} \times 2\,\mathrm{m}$

    2. Military map centred on Perdigão site, on a regularly spaced $10\,\mathrm{m} \times 10\,\mathrm{m}$

    3. SRTM map centred on Perdigão site, on a regularly spaced $30\,\mathrm{m} \times 30\,\mathrm{m}$

340 **Computational meshes** :

    1. Mesh 1: $20\,\mathrm{m} \times 20\,\mathrm{m}$

    2. Mesh 2: $40\,\mathrm{m} \times 40\,\mathrm{m}$

3. Mesh 3: $80\,\mathrm{m} \times 80\,\mathrm{m}$

Author contributions. José M.L.M. Palma conceived, coordinated and was responsible for both the work and the manuscript writing. Carlos

345   A.M. Silva carried out the fluid flow calculations, under the guidance of Vitor M.C. Gomes and Alexandre Silva Lopes. Teresa Simões and Paula Costa developed the algorithm for building identification. Vasco T.P. Batista contributed by processing the terrain data using the LAStools software.

Competing interests. No competing interests are present

Acknowledgements. The Perdigão-2017 field campaign was primarily funded by the US National Science Foundation, European Commis-

350   sion (ENER/FP7/618122/NEWA), Danish Energy Agency, German Federal Ministry of Economy and Energy, FCT-Portuguese Foundation for Science and Technology (NEWA/1/2014), and US Army Research Laboratory. We are grateful to the municipality of Vila Velha de Ródão, landowners who authorized installation of scientific equipment in their properties, the residents of Vale do Cobrão, Foz do Cobrão, Alvaiade, Chão das Servas and local businesses who kindly contributed to the success of the campaign. The campaign would not have been possible without the alliance of many persons and entities, too many to be listed here and to whom we are also grateful.

References

J. Alves. Perdigão terrestrial survey (tower 20/tse04). Technical report, Low Edge Consult Lda, Portugal, 4 2018. Terrestrial survey around tower 20/tse04, by Low Edge Consult Lda, under contract.

J. P. D. B. Carvalho. Stationarity periods during the Perdigão campaign. Master's thesis, Faculty of Engineering of the University of Porto, 2019.

F.A. Castro, J.M.L.M. Palma, and A. Silva Lopes. Simulation of the Askervein flow. Part 1: Reynolds averaged Navier-Stokes equations ($k - \varepsilon$ turbulence model). *Boundary-Layer Meteorology*, 107:501–530, 2003. https://doi.org/10.1023/A:1022818327584. URL http://dx.doi.org/10.1023/A:1022818327584.

Y. Deng, J. P. Wilson, and B. O. Bauer. DEM resolution dependencies of terrain attributes across a landscape. *International Journal of Geographical Information Science*, 21(2):187–213, January 2007. ISSN 1365-8816, 1362-3087. https://doi.org/10.1080/13658810600894364. URL http://www.tandfonline.com/doi/abs/10.1080/13658810600894364.

J.D. DeWitt, T.A. Warner, and J.F. Conley. Comparison of DEMS derived from USGS DLG, SRTM, a statewide photogrammetry program, ASTER GDEM and LiDAR: implications for change detection. *GIScience & Remote Sensing*, 52(2):179–197, March 2015. ISSN 1548-1603, 1943-7226. https://doi.org/10.1080/15481603.2015.1019708. URL http://www.tandfonline.com/doi/full/10.1080/15481603.2015.1019708.

DGT. ReNEP: The Portuguese Network of Continuously Operating Reference Stations Status, Products and Services (In Portuguese), 2017. URL http://renep.dgterritorio.gov.pt.

M. Diebold, C. Higgins, J. Fang, A. Bechmann, and M. B. Parlange. Flow over hills: A large-eddy simulation of the Bolund case. *Boundary-Layer Meteorology*, 148(1):177–194, July 2013. ISSN 0006-8314, 1573-1472. https://doi.org/10.1007/s10546-013-9807-0. URL http://link.springer.com/article/10.1007/s10546-013-9807-0.

ESRI. ArcGIS Desktop: Release 10.4. techreport, Environmental Systems Research Institute, Redlands, CA, February 2016.

T.G. Farr, P.A. Rosen, E. Caro, R. Crippen, R. Duren, S. Hensley, M. Kobrick, M. Paller, E. Rodriguez, L. Roth, D. Seal, S. Shaffer, J. Shimada, J. Umland, M. Werner, M. Oskin, D. Burbank, and D. Alsdorf. The Shuttle Radar Topography Mission. *Reviews of Geophysics*, 45(2), June 2007. ISSN 1944-9208. https://doi.org/10.1029/2005RG000183. URL https://agupubs.onlinelibrary.wiley.com/doi/abs/10.1029/2005RG000183.

H. J. S. Fernando, J. Mann, J.M.L.M. Palma, J. K. Lundquist, R. J. Barthelmie, M. Belo-Pereira, W. O. J. Brown, F. K. Chow, T. Gerz, C. M. Hocut, P. M. Klein, L. S. Leo, J. C. Matos, S. P. Oncley, S. C. Pryor, L. Bariteau, T. M. Bell, N. Bodini, M. B. Carney, M. S. Courtney, E. D. Creegan, R. Dimitrova, S. Gomes, M. Hagen, J. O. Hyde, S. Kigle, R. Krishnamurthy, J. C. Lopes, L. Mazzaro, J. M. T. Neher, R. Menke, P. Murphy, L. Oswald, S. Otarola-Bustos, A. K. Pattantyus, C. Veiga Rodrigues, A. Schady, N. Sirin, S. Spuler, E. Svensson, J. Tomaszewski, D. D. Turner, L. van Veen, N. Vasiljević, D. Vassallo, S. Voss, N. Wildmann, and Y. Wang. The Perdigão: Peering into Microscale Details of Mountain Winds. *Bulletin of the American Meteorological Society*, 100(5):799–819, May 2019. ISSN 0003-0007, 1520-0477. https://doi.org/10.1175/BAMS-D-17-0227.1. URL http://journals.ametsoc.org/doi/10.1175/BAMS-D-17-0227.1.

I.V. Florinsky and G.A. Kuryakova. Determination of grid size for digital terrain modelling in landscape investigations—exemplified by soil moisture distribution at a micro-scale. *International Journal of Geographical Information Science*, 14(8):815–832, December 2000. ISSN 1365-8816. https://doi.org/10.1080/136588100750022804. URL https://doi.org/10.1080/136588100750022804.

390   J. Lange, J. Mann, J. Berg, D. Parvu, R. Kilpatrick, A. Costache, J. Chowdhury, K. Siddiqui, and H. Hangan. For wind turbines in complex terrain, the devil is in the detail. *Environmental Research Letters*, 12(9):094020, 2017. ISSN 1748-9326. https://doi.org/10.1088/1748-9326/aa81db. URL http://stacks.iop.org/1748-9326/12/i=9/a=094020.

LAStools. Efficient LiDAR processing software (version 190927, academic), 2019. URL http://rapidlasso.com.

R. Mahalingam and M. J. Olsen. Evaluation of the influence of source and spatial resolution of DEMs on derivative prod-
395   ucts used in landslide mapping. *Geomatics, Natural Hazards and Risk*, 7(6):1835–1855, November 2016. ISSN 1947-5705. https://doi.org/10.1080/19475705.2015.1115431. URL https://doi.org/10.1080/19475705.2015.1115431.

B.B. Mandelbrot. How long is the coast of Britain? statistical self-similariry and fractional dimension. *Science*, 156:636–638, 1967.

B.B. Mandelbrot. *The Fractal Geometry of Nature*. W.H. Freeman and Company, New York, updated edition, 1982. ISBN 0-7167-1186-9.

J. Mann, N. Angelou, J. Arnqvist, D. Callies, E. Cantero, R. Chávez Arroyo, M. Courtney, J. Cuxart, E. Dellwik, J. Gottschall, S. Ivanell,
400   P. Kuhn, G. Lea, J. Matos, C. Rodrigues, J. Palma, L. Pauscher, A. Peña, J. Rodrigo, S. Söderberg, and N. Vasiljević. Complex terrain experiments in the new european wind atlas. *Philosophical Transactions of the Royal Society A: Mathematical Physical and Engineering Sciences*, 375:(2091):20160101, April 2017. https://doi.org/https://doi.org/10.1098/rsta.2016.0101. URL http://rsta.royalsocietypublishing.org/content/375/2091/20160101.

N. G. Mortensen, L. Landberg, I. Troen, E. L. Petersen, O. Rathmann, and M. Nielsen. WAsP utility programs. Technical Report Risø-R-
405   995(EN), Risø National Laboratory, Roskilde, Denmark, September 2004. URL http://orbit.dtu.dk/files/106312446/ris_i_2261.pdf.

V. Nikora and D. Goring. Mars topography: bulk statistics and spectral scaling. *Chaos, Solitons & Fractals*, 19(2):427 – 439, 2004. ISSN 0960-0779. https://doi.org/https://doi.org/10.1016/S0960-0779(03)00054-7. URL http://www.sciencedirect.com/science/article/pii/S0960077903000547. Fractals in Geophysics.

NIRAS. Perdigão aerial survey. Technical report, NIRAS, 4 2015. This is a report of a helicopter airborne survey delivered by NIRAS with
410   assistance from Blom TopEye in order to produce data for digital elevation model and ortho photo. This delivery includes a LiDAR point cloud, and 5cm (plus 20cm) Ortho Photo.

J.M.L.M. Palma, F.A. Castro, L.F. Ribeiro, A.H. Rodrigues, and A.P. Pinto. Linear and nonlinear models in wind resource assessment and wind turbine micro-siting in complex terrain. *Journal of Wind Engineering and Industrial Aerodynamics*, 96:2308–2326, December 2008. https://doi.org/10.1016/j.jweia.2008.03.012. URL http://www.sciencedirect.com/science/article/pii/S0167610508001037.

415   J.M.L.M. Palma, R. Menke, J. Mann, S. Oncley, J. Matos, and A. Silva Lopes. Perdigão–2017: experiment layout (Version 1). Technical report, *NEWA: New European Wind Atlas* (FCT Project number NEWA/0001/2014), August 23 2018. URL https://perdigao.fe.up.pt/experiments/3/documents/1232. Project coordinator: Danmarks Tekniske Universitet (DTU Wind).

J.M.L.M. Palma, A. Silva Lopes, V.M. Costa Gomes, C. Veiga Rodrigues, R. Menke, N. Vasiljević, and J. Mann. Unravelling the wind flow over highly complex regions through computational modeling and two-dimensional lidar scanning. *Journal of Physics: Conference Series*,
420   1222:012006, May 2019. ISSN 1742-6588, 1742-6596. https://doi.org/10.1088/1742-6596/1222/1/012006. URL https://iopscience.iop.org/article/10.1088/1742-6596/1222/1/012006.

P. J. Roache. *Verification and Validation in Computational Science and Engineering*. Hermosa Publishers, Albuquerque, USA, 1998. ISBN 0-913478-08-3.

R. Sibson. A brief description of natural neighbor interpolation. pages 21–36, June 1981. In *Interpreting Multivariate Data*, V. Barnett
425   (Editor), John Wiley and Sons, New York,.

C.A.M. Silva. Computational study of atmospheric flows over Perdigão: terrain resolution and domain size. Master's thesis, Faculty of Engineering of the University of Porto, 2018.

N. Vasiljević, J.M.L.M. Palma, N. Angelou, J.C. Matos, R. Menke, G. Lea, J. Mann, M. Courtney, L. Frölen Ribeiro, and V. M. M. G. C. Gomes. Perdigão 2015: methodology for atmospheric multi-Doppler lidar experiments. *Atmos. Meas. Tech.*, 10(9):3463–3483, September 2017. ISSN 1867-8548. https://doi.org/10.5194/amt-10-3463-2017. URL https://www.atmos-meas-tech.net/10/3463/2017/.

J Wagner, T Gerz, N Wildmann, and K Gramitzky. Long-term simulation of the boundary layer flow over the double-ridge site during the Perdigão 2017 field campaign. *Atmospheric Chemistry and Physics*, 19(2):1129–1146, January 2019. ISSN 1680-7316. https://doi.org/https://doi.org/10.5194/acp-19-1129-2019. URL https://www.atmos-chem-phys.net/19/1129/2019/acp-19-1129-2019-discussion.html.

D. Watson. *Nngride: An Implementation of Natural Neighbor Interpolation*. David Watson, P.O. Box 734, Claremont, WA 6010, Australia. edition, 1994.

N. Wood. The onset of separation in neutral, turbulent flow over hills. *Boundary-Layer Meteorology*, 76(1-2):137–164, 1995. ISSN 0006-8314. https://doi.org/10.1007/BF00710894. URL http://www.springerlink.com/content/v2412rh223072568/.

Y. Yamaguchi, A.B. Kahle, H. Tsu, T. Kawakami, and M. Pniel. Overview of Advanced Spaceborne Thermal Emission and Reflection Radiometer (ASTER). *IEEE Transactions on Geoscience and Remote Sensing*, 36(4):1062–1071, July 1998. ISSN 01962892. https://doi.org/10.1109/36.700991. URL http://ieeexplore.ieee.org/document/700991/.

W. Zhang and D. R. Montgomery. Digital elevation model grid size, landscape representation, and hydrologic simulations. *Water Resources Research*, 30(4):1019–1028, April 1994. ISSN 00431397. https://doi.org/10.1029/93WR03553. URL http://doi.wiley.com/10.1029/93WR03553.